

1 Measurement of the masses and width of the narrow orbitally  
2 excited ( $L = 1$ )  $B^0$  mesons

3 The CDF Collaboration

4 Version 0.2, September 26, 2007

5 **Abstract**

6 We report a measurement of the masses and width of the neutral orbitally  
7 excited  $B$  mesons in decays to  $B^{(*)+}\pi^-$  using  $1.7 \text{ fb}^{-1}$  of data collected by the  
8 CDF II detector at the Fermilab Tevatron. The mass and width of the narrow  $B_2^{*0}$   
9 state are measured to be  $m(B_2^{*0}) = 5739.9_{-1.8}^{+1.7}$  (stat.)  $_{-0.6}^{+0.5}$  (syst.)  $\text{MeV}/c^2$  and  
10  $\Gamma(B_2^{*0}) = 22.1_{-3.1}^{+3.6}$  (stat.)  $_{-2.6}^{+3.5}$  (syst.)  $\text{MeV}/c^2$  respectively. The mass difference  
11 between the narrow  $B_2^{*0}$  and  $B_1^0$  states is measured to be  $14.6_{-2.5}^{+2.2}$  (stat.)  $_{-0.9}^{+0.7}$   
12 (syst.)  $\text{MeV}/c^2$ , resulting in a  $B_1^0$  mass of  $5725.3_{-2.1}^{+1.6}$  (stat.)  $_{-1.1}^{+0.8}$  (syst.)  $\text{MeV}/c^2$ .  
13 This is currently the most precise mass measurement of these states and the first  
14 measurement of the  $B_2^{*0}$  width.

15 The bound states of a heavy  $b$  quark with either a light  $u$  or  $d$  quark are generically  
16 referred to as a  $B$  meson. The ground  $J^P = 0^-$  ( $B$ ) and  $1^-$  ( $B^*$ ) states are well  
17 established [1], but the spectroscopy of the excited  $B$  states has not been well studied.  
18 The first excited state of the  $B$  meson is predicted to occur when the light quark has an  
19 orbital angular momentum of  $L = 1$ . This results in two isodoublets of excited states,  
20 one with a light quark angular momentum of  $J_l = \frac{1}{2}$  and a total angular momentum  
21 of  $\mathbf{J} = 0$  ( $B_0^*$ ) or  $1$  ( $B_1$ ), and another with  $J_l = \frac{3}{2}$  and  $\mathbf{J} = 1$  ( $B_1$ ) or  $2$  ( $B_2^*$ ) [2–5]. The  
22 four states are collectively referred to as  $B^{**}$ . The  $J_l = \frac{1}{2}$  states decay to  $B^{(*)}\pi$  via an

23  $S$ -wave transition. Consequently, these states are expected to be very broad and have  
 24 not yet been observed. The  $J_l = \frac{3}{2}$  states decay to  $B^{(*)}\pi$  via a  $D$ -wave transition and  
 25 are expected to have widths of  $10 - 20 \text{ MeV}/c^2$  [3]. The decay  $B_1 \rightarrow B\pi$  is forbidden  
 26 by angular momentum and parity conservation, while both  $B_2^* \rightarrow B\pi$  and  $B_2^* \rightarrow B^*\pi$   
 27 decays are allowed. Decays to a  $B^*$  proceed as  $B^* \rightarrow B\gamma$ , where the photon is not  
 28 detected. Because of the missing photon, the observed  $B_1^0$  and  $B_2^{*0} \rightarrow B^*\pi$  peaks  
 29 are shifted to a lower mass by the  $B^* - B$  mass splitting of  $45.78 \pm 0.35 \text{ MeV}/c^2$  [1],  
 30 resulting in an expected signal structure of three narrow  $B^{**}$  resonances.

31 Previous measurements of the neutral  $B_1$  and  $B_2^*$  states have been made using  
 32 inclusive or semi-inclusive decays which did not allow for separation of the narrow  
 33 states [6–11], or were statistically limited [12]. Recently the DØ Collaboration has  
 34 reported resolving the neutral  $B_1$  and  $B_2^*$  states [13], but the width of these states was  
 35 not measured. In this Letter, we present a measurement of the masses of the two  $J_l = \frac{3}{2}$   
 36 states,  $B_1^0$  and  $B_2^{*0}$ , and a measurement of the width of the  $B_2^{*0}$  state. We reconstruct  
 37  $B^{**0}$  in  $B^+\pi^-$  and  $B^{*+}\pi^-$  decays; throughout this paper, any reference to a specific  
 38 charge state implies the charge conjugate state as well. We use data collected in  $p\bar{p}$   
 39 collisions by the CDF II Detector at the Fermilab Tevatron between February 2002  
 40 and January 2007, corresponding to a total integrated luminosity of  $1.7 \text{ fb}^{-1}$ .

41 The components of the CDF II detector [14] used for this analysis are the magnetic  
 42 spectrometer and the muon detectors. The tracking system is composed of a multi-layer  
 43 silicon microstrip detector [15] able to measure impact parameters with a resolution on  
 44 the order of  $35 \text{ } \mu\text{m}$  [16]. It is surrounded by an open-cell drift chamber (COT) [17].  
 45 Both components are located inside a 1.4 T axial magnetic field. Muons are detected  
 46 in planes of multi-wire drift chambers and scintillators [18] outside of the hadronic  
 47 and electromagnetic calorimeters, which act as absorbers. The muon detectors cover  
 48 the pseudorapidity range  $|\eta| \leq 1.0$ , where  $\eta = -\ln \tan(\theta/2)$  and  $\theta$  is the polar angle  
 49 measured from the proton direction.

50 A three-level trigger system is used for the online event selection. The important  
51 trigger components for this analysis are the Extremely Fast Tracker (XFT) [19], which  
52 finds tracks in the COT in the level 1 trigger, and the Silicon Vertex Trigger (SVT) [20],  
53 which at level 2 adds information from the silicon detector to the tracks found by the  
54 XFT. Two independent level 3 triggers are used in this analysis. The dimuon trigger  
55 [14] requires two tracks of opposite charge matched to track segments in the muon  
56 chambers, where the mass of the pair is consistent with the  $J/\psi$  mass. The displaced  
57 vertex trigger [21] requires two tracks with large impact parameters. Additionally, the  
58 intersection of the tracks must be displaced from the interaction point and a minimum  
59 transverse momentum, *i.e.* the momentum component perpendicular to the proton  
60 beam direction, is required for each track.

61 The offline reconstruction begins by reconstructing  $B^+$  candidates in the  $J/\psi K^+$ ,  
62  $\bar{D}^0 \pi^+$ , and  $\bar{D}^0 \pi^+ \pi^+ \pi^-$  decay modes with  $J/\psi \rightarrow \mu^+ \mu^-$  and  $\bar{D}^0 \rightarrow K^+ \pi^-$ . Decays  
63 of  $B^+ \rightarrow J/\psi K^+$  are reconstructed from the dimuon trigger data while decays of  
64  $B^+ \rightarrow \bar{D}^0 \pi^+ (\pi^+ \pi^-)$  are reconstructed from the displaced vertex trigger data. In all  
65 three decay modes, the tracks are constrained in a 3-D kinematic fit to the appropriate  
66 vertex topology with the  $J/\psi$  and  $\bar{D}^0$  masses constrained to the world average values [1].  
67 All tracks not used to reconstruct a  $B^+$  candidate are considered pion candidates, and  
68 their 4-momentum is added to that of the  $B^+$  candidates to form  $B^{**}$  candidates. We  
69 search for narrow resonances in the mass difference distribution of  $Q = m(B^+ \pi^-) -$   
70  $m(B^+) - M_{\pi^-}$ , where  $m(B^+ \pi^-)$  and  $m(B^+)$  are the reconstructed invariant masses of  
71 the  $B^+ \pi^-$  pair and the  $B^+$  candidate respectively, and  $M_{\pi^-}$  is the known pion mass [1].

72 Selection of the  $B^{**}$  candidates is done using separate neural networks for each of  
73 the three  $B^+$  decay modes. The neural networks are based on the NEUROBAYES [22]  
74 package and combine discriminating variables into a single quantity.

75 We build different neural networks for each of the three  $B^+$  decay modes. The  
76 neural networks for the  $B^+ \rightarrow J/\psi K^+$  and  $B^+ \rightarrow \bar{D}^0 \pi^+ \pi^+ \pi^-$  channels use simulated

77 events as the signal patterns and data events from the  $B^+$  mass sideband as the back-  
 78 ground patterns for training. In the  $B^+ \rightarrow \bar{D}^0 \pi^+$  channel, the neural network is trained  
 79 using only data. To train on data only, we take  $B^+$  candidates in the invariant mass  
 80 signal region of 5240 to 5310 MeV/ $c^2$  as the signal patterns and  $B^+$  candidates in the  
 81 invariant mass sideband region of 5325 to 5370 MeV/ $c^2$  as the background patterns.  
 82 Events from the  $B^+$  mass sideband are also used as signal patterns with a negative  
 83 weight to account for the background in the signal region. The most important topo-  
 84 logical and kinematic discriminants for the neural networks are the impact parameter  
 85 of the  $B^+$ , the projection of the distance of the  $B^+$  decay vertex to the primary vertex  
 86 on the normalized transverse momentum, the transverse momentum of the kaon or  
 87 pion from the  $B^+$  decay, and the impact parameter of the kaon or pion from the  $B^+$   
 88 decay. The neural networks for  $B^+$  selection in the  $B^+ \rightarrow J/\psi K^+$  and  $B^+ \rightarrow \bar{D}^0 \pi^+$   
 89 channels are taken from the study of the  $B_s^{**}$  states [23]. The fitted  $B^+$  yields are  
 90 51 500 in the  $J/\psi K^+$  decay channel, 40 100 in the  $\bar{D}^0 \pi^+$  channel, and 11 000 in the  
 91  $\bar{D}^0 \pi^+ \pi^+ \pi^-$  channel.

92 For the  $B^{**}$  selection, three neural networks are formulated and trained on a com-  
 93 bination of simulated events for the signal patterns and data for the background pat-  
 94 terns. The data for the background patterns are taken from the entire  $Q$  range of 0 to  
 95 1 GeV/ $c^2$ . The signal contribution in the data is marginal and can be neglected during  
 96 neural network training. To avoid biasing the network in the training, the simulated  
 97 events are generated with the same  $Q$  distribution as the data. The neural network  
 98 inputs include the output of the corresponding  $B^+$  neural network and the properties  
 99 of the pion from  $B^{**}$  decay in addition to the quantities used by the corresponding  
 100  $B^+$  neural network. The most important discriminants are the impact parameter and  
 101 transverse momentum of the pion from  $B^{**}$  decay and the output of the  $B^+$  neural  
 102 network.

103 For the final  $B^{**}$  selection we select on the number of candidates per event and on

104 the output of the neural networks. The requirement on the number of candidates is  
 105 fixed to be the same for all three  $B^+$  decay channels, and requires fewer than six  $B^{**}$   
 106 candidates in an event. The cut on the neural network output is chosen to maximize  
 107  $N_{MC}/\sqrt{N_{data}}$ . The optimization is done by counting the number of Monte Carlo events  
 108  $N_{MC}$  and the number of data events  $N_{data}$  in the  $Q$  signal region of 0.2 to 0.4  $\text{GeV}/c^2$   
 109 for a given cut on the network output. In this analysis, we combine the  $B^{**}$  events for  
 110 all three  $B^+$  decay channels and use this combined  $Q$  distribution to measure the  $B^{**}$   
 111 properties. Thus, we optimize the  $B^{**}$  selection for each  $B^+$  decay channel using the  
 112 combined significance, which is a function of all three network outputs. The resulting  
 113 combined  $Q$  distribution is shown in Figure 1.

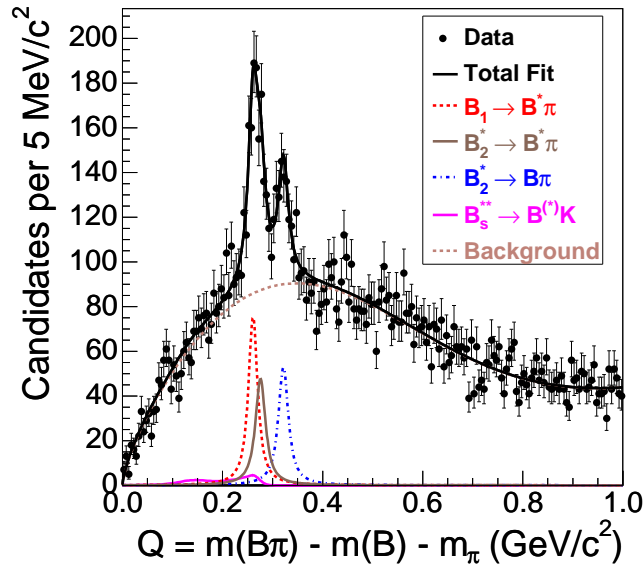


Figure 1: Invariant mass distribution  $Q = m(B^+\pi^-) - m(B^+) - M_{\pi^-}$  for exclusive  $B^+$  decays. The fit is described in the text. Curves are shown separately for the background, the  $B_s^{**}$  reflections, and the three  $B^{**}$  decays.

114 We perform an unbinned maximum-likelihood fit to the combined  $Q$  distribution.  
 115 The  $B^{**}$  signal structure is interpreted as the three decays  $B_1^0 \rightarrow B^{*+}\pi^-$ ,  $B_2^0 \rightarrow$   
 116  $B^+\pi^-$ , and  $B_2^0 \rightarrow B^{*+}\pi^-$ , with  $B^{*+} \rightarrow B^+\gamma$ . Because of the missing photon in

117 decays through  $B^*$ , we expect a total of three narrow  $B^{**}$  signal peaks. Each peak  
 118 is modeled by a non-relativistic fixed-width Breit-Wigner distribution convoluted with  
 119 the detector resolution model. The detector resolution as a function of  $Q$  is determined  
 120 from simulation and modeled by two Gaussian distributions, a dominant narrow core  
 121 of an  $\sim 2 \text{ MeV}/c^2$  width and a small broad component of an  $\sim 4 \text{ MeV}/c^2$  width for the  
 122 tails. A systematic uncertainty is assigned for possible underestimation of the detector  
 123 resolution by the simulation.

124 The current sample of data has insufficient statistics to fit for all signal parameters.  
 125 We fit for the  $Q$  value of the  $B_2^{*0} \rightarrow B^+\pi^-$  decay, the mass difference between the  
 126  $B_1^0$  and  $B_2^{*0}$  states, the width of the  $B_2^{*0}$ , and the number of events in the  $B_1^0$  and  
 127  $B_2^{*0} \rightarrow B^+\pi^-$  peaks. Other parameters are imposed as part of the fit and are taken  
 128 either from previous measurements or from theoretical predictions. These are: the  
 129 energy of the  $B^*$  photon,  $E(\gamma) = 45.78 \pm 0.35 \text{ MeV}/c^2$  [1]; the ratio of the  $B_1^0$  and  $B_2^{*0}$   
 130 widths,  $\frac{\Gamma(B_1^0)}{\Gamma(B_2^{*0})} = 0.9 \pm 0.2$  [3]; the ratio of the  $B_2^{*0}$  branching fractions,  $\frac{BR(B_2^{*0} \rightarrow B^+\pi^-)}{BR(B_2^{*0} \rightarrow B^{*+}\pi^-)} =$   
 131  $1.1 \pm 0.3$ , which is based on observations of the charm sector [11].

132 We also expect reflections from  $B_s^{**0} \rightarrow B^+K^-$  decays in the  $B^{**}$   $Q$  distribution  
 133 when the kaon is mistakenly assigned the pion mass. The shape of this reflection is  
 134 determined by using simulations from the study of the  $B_s^{**}$  states [23] and is a fixed  
 135 component of the fit. The number of  $B_s^{**0}$  events expected in the  $B^{**}$  distributions  
 136 is also determined from [23] and enter the fit as Gaussian constraints with a 50%  
 137 uncertainty assigned. In this data sample we expect 24  $B_{s1}^0$  events and 62  $B_{s2}^{*0}$  events.

138 The background is modeled by a power law times an exponential. There is a small  
 139 fixed component to the background at high  $Q$  values ( $Q > 0.7 \text{ GeV}/c^2$ ), but the  
 140 background shape under the  $B^{**}$  signal region is allowed to float in the fit to data.

141 The result of this fit to the combined data is shown in Figure 1. The  $\chi^2$  probability  
 142 of the fit is 78% in the range  $Q \in [0.0, 0.5] \text{ GeV}/c^2$ . The following parameters are

143 measured for the  $B_1^0$  and  $B_2^{*0}$ :

$$144 \quad m(B_2^{*0}) - m(B^+) - M_{\pi^-} = 321.5_{-1.8}^{+1.7} \text{ (stat.) } {}_{-0.3}^{+0.4} \text{ (syst.) MeV}/c^2,$$

$$145 \quad m(B_2^{*0}) - m(B_1^0) = 14.9_{-2.5}^{+2.2} \text{ (stat.) } {}_{-0.9}^{+0.7} \text{ (syst.) MeV}/c^2, \text{ and}$$

$$146 \quad \Gamma(B_2^{*0}) = 22.7_{-3.2}^{+3.8} \text{ (stat.) } {}_{-1.6}^{+2.1} \text{ (syst.) MeV}/c^2.$$

147 The number of events are  $N(B_1^0) = 503_{-68}^{+75}$  (stat.)  ${}_{-73}^{+86}$  (syst.),  $N(B_2^{*0} \rightarrow B^+\pi^-) =$   
 148  $385_{-45}^{+48}$  (stat.)  ${}_{-23}^{+32}$  (syst.), and  $N(B_2^{*0} \rightarrow B^{*+}\pi^-) = 351_{-45}^{+48}$  (stat.)  ${}_{-23}^{+31}$  (syst.). The  
 149 signal is consistent with theoretical predictions, including those entered as Gaussian  
 150 constraints in the likelihood. Using the mass of the  $B^+$  [1] and the correlations between  
 151 the fit parameters, the absolute masses of the  $B_1^0$  and  $B_2^{*0}$  are:

$$152 \quad m(B_2^{*0}) = 5740.2_{-1.8}^{+1.7} \text{ (stat.) } {}_{-0.5}^{+0.6} \text{ (syst.) MeV}/c^2 \text{ and}$$

$$153 \quad m(B_1^0) = 5725.3_{-2.2}^{+1.6} \text{ (stat.) } {}_{-1.1}^{+0.9} \text{ (syst.) MeV}/c^2.$$

154 Systematic uncertainties on the mass differences, width, and yield measurements  
 155 fall into three categories: mass scale, assumptions entered as Gaussian constraints in  
 156 the fit, and the choice of background and resolution models.

157 To determine the mass scale uncertainty, we compare CDF II measured  $Q$  values  
 158 of the  $D^*$ ,  $\Sigma_c^0$ ,  $\Sigma_c^{++}$ ,  $\Lambda_c^*$ , and  $\psi(2S)$  hadrons with the world average  $Q$  values [1]. We  
 159 reconstruct the decays  $D^{*+} \rightarrow D^0\pi^+$  with  $D^0 \rightarrow K^+\pi^-$ ,  $\Sigma_c^0 \rightarrow \Lambda_c^+\pi^-$ ,  $\Sigma_c^{++} \rightarrow \Lambda_c^+\pi^+$ ,  
 160 and  $\Lambda_c^{*+} \rightarrow \Lambda_c^+\pi^+\pi^-$ , all with  $\Lambda_c^+ \rightarrow pK^-\pi^+$ , and  $\psi(2S) \rightarrow J/\psi\pi^+\pi^-$  with  $J/\psi \rightarrow$   
 161  $\mu^+\mu^-$ . The  $Q$  value dependence of this systematic uncertainty is modeled with a linear  
 162 function, which is evaluated at the  $B^{**}$   $Q$  values to estimate the systematic uncertainty.  
 163 This is a small contribution to the systematic uncertainty.

164 Assumptions made in the fit are included as Gaussian constraints added to the  
 165 likelihood. Thus, the systematic uncertainty due to these assumptions is part of the fit  
 166 uncertainty on each parameter. To separate the statistical and systematic components

Table 1: Systematic uncertainties of the  $B^{**0}$  parameters. Each row corresponds to one source of systematic uncertainty. The columns show the resulting uncertainties for the five  $B^{**}$  signal parameters. Uncertainties on the mass difference and width parameters are in units of  $\text{MeV}/c^2$ .

Source	$Q(B_2^{*0})$	$\Gamma(B_2^{*0})$	$m(B_2^{*0}) - m(B_1^0)$	$N(B_2^{*0} \rightarrow B^+\pi^-)$	$N(B_1^0)$
Mass scale	+0.05 -0.05		+0.003 -0.003		
Fit constraints	+0.4 -0.3	+2.1 -1.5	+0.7 -0.9	+27 -23	+86 -72
Background parameterization	+0.14	-0.1	+0.16	+17	-13
Resolution uncertainty	+0.003	-0.5	+0.001	-2	-3
Total	+0.4 -0.3	+2.1 -1.6	+0.7 -0.9	+32 -23	+86 -73

167 of the fit uncertainty, we refit the data with the constrained parameters fixed. The  
168 uncertainty on each parameter from this fit is purely statistical. To determine the  
169 systematic contribution to the fit uncertainty, we subtract in quadrature the uncer-  
170 tainties for the two fits to data, one with the constrained parameters floating and one  
171 with them fixed. Assumptions in the fit are the largest systematic uncertainty on all  
172 parameters.

173 To estimate the uncertainty due to the choice of background or resolution models,  
174 we generate pseudo-experiments using an alternate background parameterization or  
175 increased resolution width. Each pseudo-experiment is modeled by both the default  
176 fit and the fit with an alternate background model or increased resolution width. We  
177 then take the difference between the parameter values in the varied fit and the default  
178 fit as the systematic uncertainty due to the model. We fit the distribution of pseudo-  
179 experiment differences with a Gaussian, and take the mean of the Gaussian as the  
180 systematic uncertainty. The uncertainty due to the detector resolution underestimation  
181 is negligible. The uncertainty due to the background model is also relatively small.

182 In summary, using the three fully reconstructed decay modes  $B^{**0} \rightarrow B^+\pi^- \rightarrow$   
183  $(J/\psi K^+)\pi^-$ ,  $B^{**0} \rightarrow B^+\pi^- \rightarrow (\bar{D}^0\pi^+)\pi^-$ , and  $B^{**0} \rightarrow B^+\pi^- \rightarrow (\bar{D}^0\pi^+\pi^+\pi^-)\pi^-$ ,  
184 we observe the two narrow  $B^{**0}$  states in agreement with previous measurements and

185 theoretical predictions. This is the most precise measurement of the narrow  $B^{**0}$  states  
186 to date. This is also the first measurement of the  $B_2^{*0}$  width.

187 We thank the Fermilab staff and the technical staffs of the participating institu-  
188 tions for their vital contributions. This work was supported by the U.S. Department of  
189 Energy and National Science Foundation; the Italian Istituto Nazionale di Fisica Nu-  
190 cleare; the Ministry of Education, Culture, Sports, Science and Technology of Japan;  
191 the Natural Sciences and Engineering Research Council of Canada; the National Sci-  
192 ence Council of the Republic of China; the Swiss National Science Foundation; the  
193 A.P. Sloan Foundation; the Bundesministerium für Bildung und Forschung, Germany;  
194 the Korean Science and Engineering Foundation and the Korean Research Foundation;  
195 the Science and Technology Facilities Council and the Royal Society, UK; the Institut  
196 National de Physique Nucleaire et Physique des Particules/CNRS; the Russian Founda-  
197 tion for Basic Research; the Comisión Interministerial de Ciencia y Tecnología, Spain;  
198 the European Community's Human Potential Programme; the Slovak R&D Agency;  
199 and the Academy of Finland.

## 200 References

- 201 [1] W. M. Yao *et al.* (Particle Data Group), *J. Phys. G* **33**, 1 (2006).
- 202 [2] E. J. Eichten, C. T. Hill, and C. Quigg, *Phys. Rev. Lett.* **71**, 4116 (1993);  
203 E. J. Eichten, C. T. Hill, and C. Quigg, FERMILAB-CONF-94/118-T (1994).
- 204 [3] A. F. Falk and T. Mehen, *Phys. Rev. D* **53**, 231 (1996).
- 205 [4] N. Isgur, *Phys. Rev. D* **57**, 4041 (1998).
- 206 [5] D. Ebert, V. O. Galkin, and R. N. Faustov, *Phys. Rev. D* **57**, 5663 (1998)  
207 [Erratum-*ibid.* *D* **59**, 019902 (1999)].

- 208 [6] R. Akers *et al.* (OPAL Collaboration), *Z. Phys. C* **66**, 19 (1995).
- 209 [7] P. Abreu *et al.* (DELPHI Collaboration), *Phys. Lett. B* **345**, 598 (1995).
- 210 [8] D. Buskulic *et al.* (ALEPH Collaboration), *Z. Phys. C* **69**, 393 (1996).
- 211 [9] M. Acciarri *et al.* (L3 Collaboration), *Phys. Lett. B* **465**, 323 (1999).
- 212 [10] A. A. Affolder *et al.* (CDF Collaboration), *Phys. Rev. D* **64**, 072002 (2001).
- 213 [11] Z. Albrecht *et al.* (DELPHI Collaboration), DELPHI 2004-025 CONF 700,  
214 contributed paper to ICHEP 2004, Beijing.
- 215 [12] R. Barate *et al.* (ALEPH Collaboration), *Phys. Lett. B* **425**, 215 (1998).
- 216 [13] V. M. Abazov *et al.* (D0 Collaboration), arXiv:0705.3229 [hep-ex].
- 217 [14] D. Acosta *et al.* (CDF Collaboration), *Phys. Rev. D* **71**, 032001 (2005).
- 218 [15] C. S. Hill, *Nucl. Instrum. Methods A* **530**, 1 (2004); A. Affolder *et al.*, *Nucl.*  
219 *Instrum. Methods A* **453**, 84 (2000); A. Sill, *Nucl. Instrum. Methods A* **447**,  
220 1 (2000).
- 221 [16] A. Bardi *et al.*, *Nucl. Instrum. Methods Phys. Res. A* **485**, 178 (2002).
- 222 [17] T. Affolder *et al.*, *Nucl. Instrum. Methods A* **526**, 249 (2004).
- 223 [18] G. Ascoli *et al.*, *Nucl. Instrum. Methods A* **268**, 33 (1988).
- 224 [19] E. J. Thomson *et al.*, *IEEE Trans. Nucl. Sci.* **49**, 1063 (2002).
- 225 [20] W. Ashmanskas *et al.*, *Nucl. Instrum. Methods A* **518**, 532 (2004).
- 226 [21] A. Abulencia *et al.* (CDF Collaboration), *Phys. Rev. Lett.* **96**, 191801 (2006).

- 227 [22] M. Feindt, arXiv:physics/0402093 (2004); M. Feindt and U. Kerzel, Nucl. In-  
228 strum. Methods A **559**, 190 (2006).
- 229 [23] CDF Collaboration, “Observation of orbitally excited  $L = 1$   $B_s$  mesons”, CDF  
230 Note 8468 (2006).